Fracture in mode I using a conserved phase-field model

L. O. Eastgate, J. P. Sethna, M. Rauscher, and T. Cretegny

Laboratory of Atomic and Solid State Physics, Cornell University, Ithaca, New York 14853

C.-S. Chen and C. R. Myers

Cornell Theory Center, Cornell University, Ithaca, New York 14853

We present a continuum phase-field model of crack propagation. It includes a phase-field that is proportional to the mass density and a displacement field that is governed by linear elastic theory. Generic macroscopic crack growth laws emerge naturally from this model. In contrast to classical continuum fracture mechanics simulations, our model avoids numerical front tracking. The added phase-field smooths the sharp interface, enabling us to use equations of motion for the material (grounded in basic physical principles) rather than for the interface (which often are deduced from complicated theories or empirical observations). The interface dynamics thus emerges naturally. In this paper, we look at stationary solutions of the model, mode I fracture, and also discuss numerical issues. We find that the Griffith's threshold underestimates the critical value at which our system fractures due to long wavelength modes excited by the fracture process.

I. INTRODUCTION

The study of fracture is usually approached using mathematical descriptions and numerical simulations based on empirical observations. Finite element methods are commonly used to investigate the behavior of fractured materials on a large scale, where the crack growth laws [1,2] (that is, velocity and direction of the crack for a given stress field near the tip) are introduced empirically.

We present a continuum description starting from basic theoretical assumptions. We introduce a phase-field model, originally used to describe thermodynamic phase transitions and widely used to model solidification [3], and combine it with a displacement field. In contrast to other phase-field models of fracture [4,5] and interfacial motion in the presence of strain [6,7], our phase-field is conserved, representing the density of the material. Bhate *et al.* [8] study a conserved order-parameter phase-field model in the context of stress voiding in electromigration; their dynamics is rather different from ours, since their elastic deformations are quasistatically relaxed (the limit in our theory of $\eta \rightarrow 0$, see below).

The phase-field serves two main purposes. First, it smears out any sharp interfaces, facilitating numerical convergence. Second, the model gives equations of motion for the material rather than the boundaries, thus we avoid dealing with a moving boundary value problem which would require numerical front tracking. One of our main goals is to find macroscopic fracture laws. In our model, these laws emerge naturally from the dynamics of the fields. See Fig. 1 for a three dimensional representation of the phase-field in a fracturing sample.

One incentive to use a conserved-order parameter is simply that density is conserved microscopically (apart from applications where etching or sublimation is important). In general, a nonconserved phase-field will give a nonzero velocity even for a straight material interface [4]. This could be remedied by tuning the free energy so that the material and vacuum have the same energy density, but then the strained

region around the crack tip would evaporate. Conserving the phase-field also gave us insight into how to properly implement the conservation laws (see Sec. II). Another option would have been to add a nonconserved field, such as damage or dislocation density, in addition to our conserved mass. This would add complexity without ameliorating the numerical challenges presented by the conservation law. In future work we intend to introduce such nonconserved state variables to model plastic flow.

Section II gives an outline of the theoretical model, presenting the main equations. We then investigate some of the stationary solutions analytically, and discuss their consequences. This is followed by a brief presentation of the numerical implementation. We then measure the crack growth velocity as a function of external stress and explore the fracture threshold of our model. We conclude with suggestions for future work.

II. THE FRACTURE MODEL

The model consists of a phase-field ϕ and a displacement field **u**. The former field is interpreted as the normalized
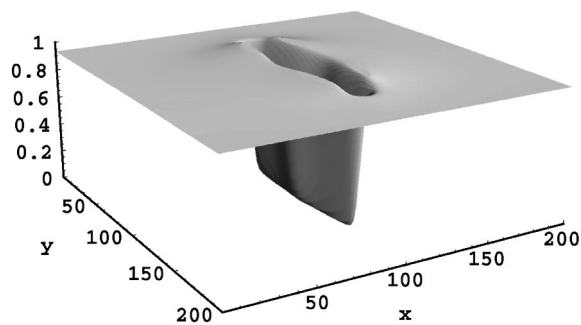

FIG. 1. A three-dimensional representation of the phase-field in a fracturing sample. The vertical axis shows the value of the phase-field $\phi(x,y)$, where $\phi=1$ is unstrained material and $\phi=0$ is vacuum. This example corresponds to the fourth contour in Fig. 4. The values of x and y are given in units of w/h (see Appendix A).

mass density, and typically has values between zero and one. The latter field, through its derivatives, represents strain in the material. The model is based on a free energy $\mathcal{F}$. The equations of motion locally conserve the density ϕ, moves it under the flow field $\mathbf{u}$, and evolves both ϕ and $\mathbf{u}$ in the direction of the net force from the free energy: in particular they are constructed so that $d\mathcal{F}/dt < 0$. The free energy is given by the integral

$$\mathcal{F} = \int \left(\frac{w^2}{2} |\boldsymbol{\nabla} \phi|^2 + g[\phi, \boldsymbol{\epsilon}] \right) dV, \tag{1}$$

where

$$g[\phi, \boldsymbol{\epsilon}] = \frac{h^2}{4} \phi^2 (\phi_s[\boldsymbol{\epsilon}] - \phi)^2 + \phi^2 \mathcal{E}[\boldsymbol{\epsilon}]. \tag{2}$$

The first term in Eq. (1) is a gradient term, energetically penalizing spatial fluctuations in the phase-field. The first term in Eq. (2) is a Ginzburg-Landau double well potential, favoring values of ϕ at zero and $\phi_s[\boldsymbol{\epsilon}] \equiv 1 - \epsilon_{mm}$ (using the Einstein summing convention), representing the two phases vacuum and solid, respectively. If the material is completely unstrained the solid value is $\phi_s[\boldsymbol{\epsilon}] \equiv 1$, otherwise this value is either higher (for a compressed material) or lower (for a stretched material), where ϵ_{mm} is the density change for small strain. The factor $\phi_s[\boldsymbol{\epsilon}] - \phi$ can be thought of as a density of vacancies or interstitials. The parameter h controls the height of the energy barrier between the vacuum and solid phases. The ratio of w and h controls the width of the solid-vacuum interface, that is the width of the transition from $\phi = \phi_s[\boldsymbol{\epsilon}]$ to $\phi = 0$.

The next term is the elastic strain energy density $\mathcal{E}[\boldsymbol{\epsilon}]$. The elastic energy is calculated from the strain tensor $\boldsymbol{\epsilon}$, and is given by

$$\mathcal{E}[\boldsymbol{\epsilon}] = \tfrac{1}{2} \sigma_{ij} \epsilon_{ij} = \tfrac{1}{2} C_{ijkl} \epsilon_{kl} \epsilon_{ij}. \tag{3}$$

For a homogeneous, isotropic material, the tensor C_{ijkl} can be described by the two Lamé constants μ and λ through

$$C_{ijkl} = \mu (\delta_{ik} \delta_{jl} + \delta_{il} \delta_{jk}) + \lambda \delta_{ij} \delta_{kl}, \tag{4}$$

where μ is the shear modulus and λ is proportional to the bulk modulus. This gives

$$\sigma_{ij} = \lambda \epsilon_{mm} \delta_{ij} + 2\mu \epsilon_{ij}. \tag{5}$$

In two dimensions, we get

$$\mathcal{E}[\boldsymbol{\epsilon}] = \frac{\lambda}{2} (\epsilon_{xx} + \epsilon_{yy})^2 + \mu (\epsilon_{xx}^2 + \epsilon_{yy}^2 + \epsilon_{xy}^2 + \epsilon_{yx}^2). \tag{6}$$

The strain field ϵ_{ij} is related to the displacement field by

$$\epsilon_{ij} = \frac{1}{2} \left(\frac{\partial u_i}{\partial x_j} + \frac{\partial u_j}{\partial x_i} \right). \tag{7}$$

Note that in this definition of the strain field, we are ignoring geometric nonlinearities [9], which are important for large rotations. According to Eq. (7), the divergence of the dis-

placement field is just the trace of the strain, $\boldsymbol{\nabla} \cdot \mathbf{u} = \epsilon_{mm}$. The displacement field $\mathbf{u}(\mathbf{x})$ is defined in the deformed or Eulerian coordinate system, which means that $\mathbf{x}$ describes a location in space. (In the undeformed or Lagrangian description, $\mathbf{x}$ would describe the location of the material before the displacement is taken into account; Lagrangian coordinates are usually used in finite element calculations.) The Lamé constants are connected through the Poisson ratio ν by $\lambda = 2\mu\nu/(1-2\nu)$, see Appendix B. In the case of plane strain, the addition of the $\boldsymbol{\nabla} \cdot \mathbf{u}$ term in the double well potential turns out to be crucial to preserve this relation. Since the elastic energy $\mathcal{E}[\boldsymbol{\epsilon}]$ is only defined in the material (that is, where $\phi \neq 0$), the elastic term is multiplied by a factor of ϕ^2; thus the strain energy will go to zero in the vacuum.

The equations of motion we have chosen for the phase-field ϕ and displacement field $\mathbf{u}$ are overdamped and Eulerian, moving the fields along the direction of net force. The time derivative is thus proportional to the force on the field. Physically, our model might describe fracture of a colloidal crystal, or ''atoms in molasses.'' We are therefore intermediate between quasistatic fracture (where the crack evolution is calculated from the static strain of the current configuration) and dynamic fracture (with inertial effects and wave reflection at the boundaries). Specifically, our equations of motion are

$$\frac{\partial \phi}{\partial t} = -\boldsymbol{\nabla} \cdot \mathbf{J} \quad \mathbf{J} = -D\boldsymbol{\nabla} \frac{\delta \mathcal{F}}{\delta \phi} + \phi \frac{\partial \mathbf{u}}{\partial t}, \tag{8a}$$

$$\frac{\partial \mathbf{u}}{\partial t} = -\frac{1}{\eta} \frac{\mathrm{D}\mathcal{F}}{\mathrm{D}\mathbf{u}} = -\frac{1}{\eta} \left(\frac{\delta \mathcal{F}}{\delta \mathbf{u}} + \phi \boldsymbol{\nabla} \frac{\delta \mathcal{F}}{\delta \phi} \right), \tag{8b}$$

where η and D are the viscosity and the diffusion constant, respectively. Note that Eq. (8a) is the continuity equation. This means that total ϕ, or mass, is conserved. The first term in $\mathbf{J}$ is a diffusion term, while the second term makes sure that the mass follows the motion of the displacement field. The total variational derivative $\mathrm{D}\mathcal{F}/\mathrm{D}\mathbf{u}$ in Eq. (8b) can be found by first noting that a small change $\Delta \mathbf{u}$ in $\mathbf{u}$ results in a change in ϕ. The new value of ϕ at a point changes due to two effects: (i) a gradient in ϕ dragged by a distance $\Delta \mathbf{u}$ changes it by $-(\boldsymbol{\nabla} \phi) \cdot (\Delta \mathbf{u})$, and (ii) a divergence in $\Delta \mathbf{u}$ causes a change in density $-\phi \boldsymbol{\nabla} \cdot (\Delta \mathbf{u})$. Together these combine into the net change $\Delta \phi[\Delta \mathbf{u}] = -\boldsymbol{\nabla} \cdot (\phi \Delta \mathbf{u})$. This is the continuity equation, where $\phi \Delta \mathbf{u}$ is the flux of ϕ. The total change in the free energy is then

$$\Delta \mathcal{F}[\Delta \mathbf{u}] = \int \left(\frac{\delta \mathcal{F}}{\delta \mathbf{u}} \cdot \Delta \mathbf{u} + \frac{\delta \mathcal{F}}{\delta \phi} \Delta \phi[\Delta \mathbf{u}] \right) dV$$

$$= \int \left[\frac{\delta \mathcal{F}}{\delta \mathbf{u}} \cdot \Delta \mathbf{u} - \boldsymbol{\nabla} \cdot (\phi \Delta \mathbf{u}) \frac{\delta \mathcal{F}}{\delta \phi} \right] dV$$

$$= \int \left(\frac{\delta \mathcal{F}}{\delta \mathbf{u}} \cdot \Delta \mathbf{u} + \phi \boldsymbol{\nabla} \frac{\delta \mathcal{F}}{\delta \phi} \cdot \Delta \mathbf{u} \right) dV$$

$$\equiv \int \left(\frac{\mathrm{D}\mathcal{F}}{\mathrm{D}\mathbf{u}} \cdot \Delta \mathbf{u} \right) dV. \tag{9}$$

We assume that the boundary terms vanish in the integration by parts.

With the equations of motion (8), the evolution of the fields are overdamped and the free energy decreases in time

$$\frac{d}{dt}\mathcal{F} = \int \left(\frac{\delta\mathcal{F}}{\delta\phi}\frac{\partial\phi}{\partial t} + \frac{\delta\mathcal{F}}{\delta\mathbf{u}}\frac{\partial\mathbf{u}}{\partial t} \right) dV$$

$$= \int \left\{ \frac{\delta\mathcal{F}}{\delta\phi}\left[D\nabla^2\frac{\delta\mathcal{F}}{\delta\phi} - \nabla\cdot\left(\phi\frac{\partial\mathbf{u}}{\partial t} \right) \right] + \frac{\delta\mathcal{F}}{\delta\mathbf{u}}\frac{\partial\mathbf{u}}{\partial t} \right\} dV$$

$$= \int \left[-D\left(\nabla\frac{\delta\mathcal{F}}{\delta\phi} \right)^2 + \frac{\partial\mathbf{u}}{\partial t}\cdot\left(\phi\nabla\frac{\delta\mathcal{F}}{\delta\phi} + \frac{\delta\mathcal{F}}{\delta\mathbf{u}} \right) \right] dV$$

$$= \int \left[-D\left(\nabla\frac{\delta\mathcal{F}}{\delta\phi} \right)^2 - \eta\left(\frac{\partial\mathbf{u}}{\partial t} \right)^2 \right] dV \leq 0. \qquad (10)$$

To solve for the fields, the functional derivatives need to be calculated explicitly. They can be written in the convenient form

$$\frac{\delta\mathcal{F}}{\delta u_i} = -\partial_j\left[\frac{\partial g}{\partial\epsilon_{ij}} \right], \qquad (11a)$$

$$\frac{\delta\mathcal{F}}{\delta\phi} = -w^2\nabla^2\phi + \frac{\partial g}{\partial\phi}. \qquad (11b)$$

Finally, it should be pointed out that all the equations can be made unitless by rescaling all the quantities involved. For the present model it is convenient to use w/h as the unit length, h^2 as the unit energy density, and $1/\eta$ as the unit diffusivity. This corresponds to setting $w=1$, $h=1$, and $\eta=1$ in Eqs. (1), (8b), and (11). See Appendix A for information on reduced units for the quantities used in this paper.

III. STATIONARY SOLUTION

This section will calculate the profile of a stationary straight interface between the solid and vacuum phases. Before delving into the details, consider Eqs. (8). A stationary solution means that $\dot{\phi}=0$ and $\dot{\mathbf{u}}=0$. Unless we have the trivial solution where ϕ is constant, this implies that $\nabla[\delta\mathcal{F}/\delta\phi]=0$ and $\delta\mathcal{F}/\delta\mathbf{u}=0$. Physically $\delta\mathcal{F}/\delta\phi$ can be considered a chemical potential, and a nonzero gradient will result in a flow of material. This means that the chemical potential p is a constant. Thus to find a stationary solution, we have to require that

$$\frac{\delta\mathcal{F}}{\delta\phi} = p$$

and   (12)

$$\frac{\delta\mathcal{F}}{\delta\mathbf{u}} = 0.$$

We will find the stationary solution of a single straight interface running perpendicular to the x direction between the solid and the vacuum. We will therefore assume that ϕ

and ϵ_{xx} only vary with respect to x, that ϵ_{yy} is constant, and that $\epsilon_{xy}=\epsilon_{yx}=0$. Combining Eqs. (1) and (11) with the requirement in Eq. (12), we get

$$\partial_x^2\phi - \frac{\partial g}{\partial\phi} + p = 0, \qquad (13a)$$

$$\partial_x\frac{\partial g}{\partial\epsilon_{xx}} = 0, \qquad (13b)$$

$$\partial_y\frac{\partial g}{\partial\epsilon_{yy}} = 0. \qquad (13c)$$

Integrating Eq. (13b) gives

$$\frac{\partial g}{\partial\epsilon_{xx}} = C. \qquad (14)$$

For nonzero C, the vacuum phase ($\phi\approx0$) can be shown to be unstable, so to get an interface we must set $C=0$. Solving Eq. (14) with respect to ϵ_{xx} gives

$$\epsilon_{xx} = (1-A)[1-\phi-(1+2\lambda)\epsilon_{yy}], \qquad (15)$$

where

$$A = \frac{\lambda+2\mu}{\lambda+2\mu+1/2}. \qquad (16)$$

Next we multiply Eq. (13a) with $\partial_x\phi$. Using Eq. (14) and remembering that $\partial_x\epsilon_{yy}=0$, we can then rewrite Eq. (13a) as

$$\partial_x\left[\tfrac{1}{2}(\partial_x\phi)^2 - g[\phi,\epsilon] + p\phi \right] = 0. \qquad (17)$$

Upon integration, this becomes

$$\tfrac{1}{2}(\partial_x\phi)^2 - T[\phi] = 0, \qquad (18)$$

where

$$T[\phi] = g[\phi,\epsilon[\phi]] - p\phi - q, \qquad (19)$$

q is the constant of integration, and Eq. (15) has been used to write $g[\phi,\epsilon]$ as a function of ϕ only (ϵ_{yy} is considered a constant). Here $T[\phi]$ can have two minima, giving the solid and vacuum densities.

Notice that Eq. (18) looks like the Hamiltonian of a classical particle at position ϕ and time x, where the first term is the kinetic energy and $-T[\phi]$ is the potential energy. If we want a solution that starts at a small and constant ϕ at $x=-\infty$, and ends at a larger constant ϕ at $x=\infty$, then $T[\phi]$ must have two stationary points with respect to ϕ, and these two points must have the same value. Since $T[\phi]$ is fourth order in ϕ, it can be written in the general form [10]

$$T[\phi] = \frac{B^2}{2}(\phi-\phi_1)^2(\phi-\phi_2)^2. \qquad (20)$$

Comparing this to Eqs. (2) and (19), we find that [11] $B^2=A/2$ and
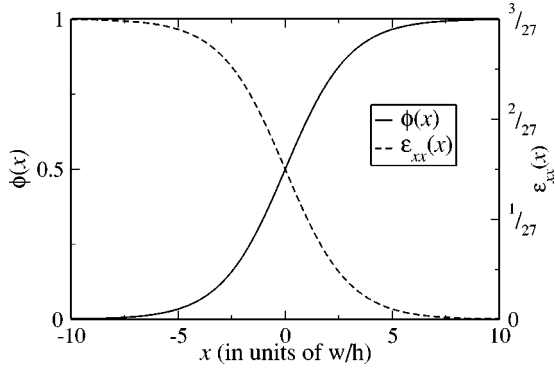
FIG. 2. A plot showing the stationary solution when $\epsilon_{yy}=0$, with $\lambda=2\mu=2$ and $c=0$. Note that the strain $\epsilon_{xx}(x)$ remains at nonzero as $\phi(x)\to 0$; this is acceptable, since the strain does not contribute to the free energy in this limit (this is not true when $\epsilon_{yy}\ne 0$).

$$\phi_{1,2}=\frac{A-\kappa\epsilon_{yy}\pm\sqrt{(A-\kappa\epsilon_{yy})^2-\dfrac{2\kappa(2A-\kappa)}{1-A}\epsilon_{yy}^2}}{2A},$$

(21)

where

$$\kappa=A(1+2\lambda)-2\lambda.$$ (22)

To second order in ϵ_{yy} this gives

$$\phi_1\approx\frac{\kappa(2A-\kappa)}{2A^2(1-A)}\epsilon_{yy}^2,$$ (23a)

$$\phi_2\approx 1-\frac{\kappa}{A}\epsilon_{yy}-\frac{\kappa(2A-\kappa)}{2A^2(1-A)}\epsilon_{yy}^2.$$ (23b)

Note that $\epsilon_{yy}=0$ gives $\phi_1=0$ and $\phi_2=1$.

Inserting Eq. (20) into Eq. (18) and solving for ϕ gives

$$\phi=\delta\tanh[\delta B(x-c)]+\phi_0,$$ (24)

where

$$\delta=\frac{\phi_2-\phi_1}{2},\qquad \phi_0=\frac{\phi_2+\phi_1}{2},$$ (25)

and the constant of integration c determines the location of the interface. In Fig. 2 we plot ϵ_{xx} and ϕ as a function of position according to Eqs. (15) and (24) for $\lambda=2\mu=2$, $c=0$, and $\epsilon_{yy}=0$.

Notice that the form of Eq. (20) implies

$$p=2B^2\phi_0\phi_1\phi_2$$

and

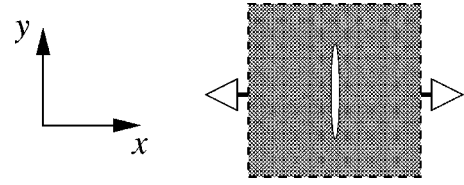(26)

$$q=-\frac{B^2}{2}\phi_1^2\phi_2^2.$$

FIG. 3. A strained material with a double-ended crack. The hollow arrows indicate the loading direction and the dashed lines are the periodic boundaries.

Consider a sample that is $\mathcal{X}$ wide and $\mathcal{Y}$ tall, with an interface perpendicular to the x direction. Let $\mathcal{X}=\mathcal{X}_1+\mathcal{X}_2$, where $\mathcal{X}_1$ is the amount of the sample that has $\phi<\phi_0$ (vacuum), and $\mathcal{X}_2$ corresponds to $\phi>\phi_0$ (solid). Then the free energy per unit length is

$$\mathcal{F}/\mathcal{Y}=\int_{\mathcal{X}}\frac{1}{2}(\partial_x\phi)^2+g[\phi,\epsilon]dx=\int_{\mathcal{X}}2T[\phi]+p\phi+q\,dx$$

$$\approx\frac{4}{3}\delta^3 B+p(\phi_1\mathcal{X}_1+\phi_2\mathcal{X}_2)+q\mathcal{X}.$$ (27)

The approximation is valid if the interface is far away from the boundaries of the sample, which means that $\mathcal{X}_{1,2}\gg 1/\delta B$.

As a prelude to the section on numerical implementation, we should point out some shortcomings of the current definition of the free energy. As seen above, the limiting value of ϕ in the vacuum side of the interface is not zero if $\epsilon_{yy}\ne 0$. Strictly speaking, there is no longer a vacuum, but a gas filling the voids of the cracks. What makes this troublesome is that this "gas" can support shear forces. We have therefore chosen to do the numerical simulations using $\epsilon_{yy}=0$ when measuring the fracture threshold. To improve the model for more complex runs, the free energy could be adjusted to assure that the value of ϕ in the limit of no material is zero for all stationary solutions.

IV. NUMERICS

A. Implementation

We have implemented Eqs. (11) for a plane strain system. Thus we can perform our simulations on a two-dimensional uniform structured grid with periodic boundary conditions in both directions. The periodic boundary conditions allows the use of Fourier methods. To increase stability, we implemented a semi-implicit scheme [12]. The linear terms can be solved analytically in Fourier space, which increases efficiency considerably. Specifically, at each time step we first integrate the nonlinear terms using an explicit Euler scheme before multiplying with the factor $\exp(-dt\nabla_{\mathbf{k}}^4)$, where $\nabla_{\mathbf{k}}^2$ is the discrete version of the Laplace operator in $\mathbf{k}$ space. In our case, this operator is equal to $\nabla_{\mathbf{k}}^2=\Sigma_{i=1,2}\{[2\cos(k_i\Delta x_i)-1]/(\Delta x_i)^2\}$. The exponential factor represents the analytical solution to the linear part of the time derivative, $\dot\phi=-\nabla^4\phi$.

In Fig. 3 we show the setup for a double-ended crack under mode I loading that we use in our numerical simulations. (See Fig. 1 for a three-dimensional representation.)

The system is initially strained in the x direction (the horizontal direction in Fig. 3) with a uniform constant strain ϵ_{xx}. Numerically, the strain is represented through the spatial derivatives of the displacement field **u**, which means that there is an inherent discontinuity in the strain field at the left and right boundary in Fig. 3. This problem has been resolved using ''skew-periodic'' boundary conditions. In essence, we identify **u** on the left with $\mathbf{u} + \Delta \mathbf{u}$ on the right.

The initial phase-field is set to the constant value that minimizes the free energy for the uniform initial strain. A circular hole is inserted into the middle by removing mass (that is, by tapering the phase-field to zero) in a circular area in the center. A crack will grow if the strain exceeds the fracture threshold. We will later compare this threshold to the Griffith's criterion.

The fourth-order gradients in our evolution equations (8) make this problem numerically challenging: most simple algorithms will become unstable at a time step which goes as the fourth power of the grid spacing. Roughly speaking, the time step must remain smaller than the time it takes information to pass across the footprint of the numerical stencil (the size of the region used to calculate the gradient terms). To make for an efficient algorithm, we paid careful attention to minimizing this footprint area: in so doing, we found that it was important to pay close attention to the locations of the various terms with respect to the numerical grid. (For example, the asymmetric forward derivative of the phase-field is located at the midpoint of the bond between two grid points). Reference [13] contains further details and suggestions. Notice that the footprint was also reduced through our use of the semi-implicit scheme mentioned earlier, leaving only third-order gradients to be solved numerically.

B. Results

Consider a block of material with a small flaw in it. If an increasing strain is applied, then at a certain point the material will fail, and a crack will form. Griffith [14] suggested that this would happen when the strain energy released is just enough to form the two newly created crack surfaces. Below we explore how our numerical simulations compare with Griffith's simple model.

In most materials, the actual fracture threshold (that is, the strain energy at which the material fractures) is higher than the Griffith's threshold. The reason is that the strain energy is converted not only to surface energy, but also to plastic deformation, sound emission, and heat. Our model has no plastic deformation, but we will see that some of the strain energy is lost through long wavelength emission similar to that of phonons in dynamic fracture.

When measuring the fracture threshold experimentally, the load or displacement on a specimen is monotonically increased until it breaks. This is difficult to do in our simulations, so instead we run a series of simulations, each with a different strain as the initial condition. We then measure the crack tip velocity as a function of strain energy per unit length stored in front of the crack, and define the fracture threshold as the energy where the velocity extrapolates to zero.
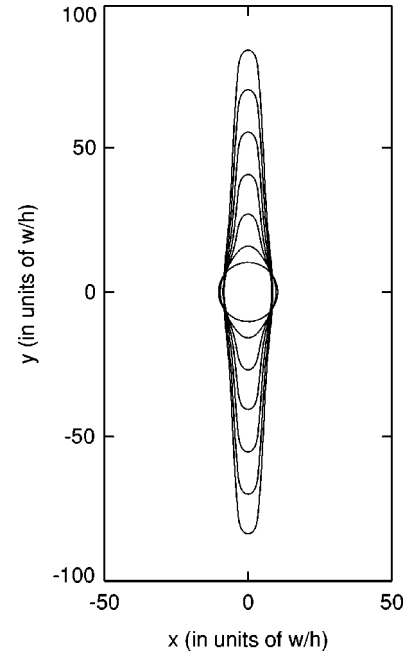

FIG. 4. A section of the system showing the $\phi=0.5$ level sets at equally spaced time intervals. The circle in the middle is the initial ''crack.'' After an initial slow transient the crack reaches a constant velocity. When it reaches the boundary and senses its periodic image, the speed will increase again as the two tips coalesce and form a continuous crack in the y direction (not shown here). This simulation corresponds to the data point in Fig. 5 with $(\mathcal{F}/\mathcal{Y})_{\text{strain}} \approx 1$ and $v \approx 0.03$.

To measure the crack tip velocity we simulated a double ended crack (see Fig. 3) on an $(\mathcal{X}, \mathcal{Y}) = (200,200)$ grid ($\Delta x = \Delta y = 1$) with periodic boundary conditions. The Lamé constants were chosen as $\lambda = 2\mu = 2$, which corresponds to $\nu = 1/3$. Initially, each simulation was given a uniform strain ϵ_{xx} in the x direction and no strain $\epsilon_{yy} = 0$ in the y direction. The phase-field ϕ was uniformly set to the value that minimizes the free energy integrand in Eq. (1) for a constant strain [15]:

$$\phi = \tfrac{3}{4}\phi_s[\epsilon] + \tfrac{1}{4}\sqrt{\phi_s^2[\epsilon] - 32\mathcal{E}[\epsilon]}. \qquad (28)$$

To initiate the crack, a circular hole of radius 10 was inserted into the center of the sample; here, a ''hole'' means that we set ϕ to zero, being careful to make the edges smooth in order to avoid numerical instabilities. After an initial transient period, the crack would start to grow in the y direction at a uniform rate until it reached the boundaries. Here, the crack would sense its periodic image and speed up as the two crack tips coalesced. Figure 4 shows part of the grid with the $\phi=0.5$ contours as the double ended crack grows in the y direction.

To measure the crack tip velocity, we needed to track the crack tip. It turns out that the free energy density has a peak in the tip area, so we decided to define the location of this peak as the crack tip position. The velocity could then be easily found by finding the slope of the curve describing the crack tip position as a function of time (we used the tip
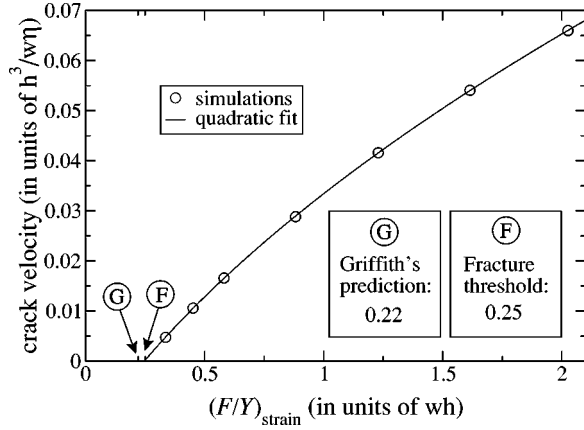
FIG. 5. The graph shows the crack tip velocity against the strain energy per unit length $(\mathcal{F}/\mathcal{Y})_{\text{strain}}$ in front of the crack tip. The simulations were done with double ended cracks in a sample of size $\mathcal{X}=\mathcal{Y}=200$, with $\lambda=2\mu=2$ and an initial strain in the y direction $\epsilon_{yy}=0$. The extrapolation of the velocity brings it to zero at a strain energy of about $(\mathcal{F}/\mathcal{Y})_{\text{strain}}=0.247\pm0.003$, as compared to the theoretical Griffith's threshold of $(\mathcal{F}/\mathcal{Y})_{\text{surface}}=2/9\approx0.222$.

growing in the positive y direction in Fig. 4). Figure 5 shows a plot of the crack tip velocity as a function of the energy per unit length $(\mathcal{F}/\mathcal{Y})_{\text{strain}}$ in the uncracked region.

A quadratic fit of $(\mathcal{F}/\mathcal{Y})_{\text{strain}}$ as a function of the crack velocity shows that the fracture threshold is $(\mathcal{F}/\mathcal{Y})_{\text{strain}}=0.247\pm0.003$.

A comment should be made about our use of periodic boundary conditions. Unlike the case of dynamical fracture, our overdamped dynamics do not suffer from elastic fields reflected from the boundaries or impinging from periodic images. However, the periodic boundary conditions do have important effects. As mentioned above, the velocity of the crack tip changes when the periodic images of the crack become sufficiently close to each other. In addition, for sufficiently thin systems (small width in the x direction) and low strains ($v\approx0$), the energy released due to the Poisson ratio is enough to favor a crack growing in the horizontal direction, parallel to the x axis (limiting how thin we can make our rectangular region). We have minimized the effects due to the periodic boundary conditions by using a wide system and by only measuring the crack velocity when the tip is far from the boundaries, although further measures might be needed for more sophisticated simulations. Note that periodic boundary conditions make it hard to apply stresses to the system; all the simulations presented in this paper were driven by applying an initial strain (equivalent to applying a displacement).

Equation (27) gives the analytical surface energy of a stationary interface. With $\epsilon_{yy}=0$, $\lambda=2\mu=2$, the total free energy per length far behind the crack tip due to the two interfaces is [16] $(\mathcal{F}/\mathcal{Y})_{\text{surface}}=2/9\approx0.222$. If our model were to obey the one proposed by Griffith, the crack tip velocity should tend to zero as $(\mathcal{F}/\mathcal{Y})_{\text{strain}}$ approaches $(\mathcal{F}/\mathcal{Y})_{\text{surface}}$. Apparently, there is a disparity between the numerical fracture threshold and the analytical Griffith's threshold for our model. Most of the energy in front of the crack tip is transferred to the newly created crack surfaces, but some extra

energy is needed to drive the crack forward.

Upon investigation, we find a large residual strain ϵ_{yy} building up across the width of the sample near the height of the crack tip during fracture. In front of the crack, the material has contracted in the y direction, presumably because of the Poisson ratio and the positive strain perpendicular to the crack. Behind the crack, the material has been stretched in the y direction; this is necessary to make up for the compressed material in front of the crack.

It turns out that the difference in energy between the fracture threshold and Griffith's threshold roughly matches the residual energy stored in this deformation. Typically, viscous effects vanish as the tip velocity goes to zero, but we claim that this one goes to a constant because the width of the deformation diverges in the limit of a stationary crack tip. Below we will give a crude analytical argument to show that this is not a finite size or finite velocity effect, and give a rough estimate of the missing energy.

Consider an infinitely long system in the y direction, but with a fixed width $\mathcal{X}$. To make the system one dimensional, we will ignore any variations in x. Here we introduce a frame that is stationary with respect to the crack tip, $\tilde{y}=y-vt$ and $\tilde{t}=t$, which means that $\partial_t\rightarrow-v\,\partial_{\tilde{y}}$ since any derivatives with respect to $\tilde{t}$ disappear for a stationary solution.

Both far in front of and far behind the tip we assume that $\epsilon_{yy}=0$, which means that the displacement field $u_y(\tilde{y})$ is constant in these areas. In the deformed region inbetween (that is, where the crack tip is), the displacement field changes by a value $\Delta u_y=u_y(-\infty)-u_y(\infty)$ (notice that the displacement field has a lower value in front of the tip). According to Eq. (5), the strain far ahead of the tip exerts a stress

$$\sigma_{yy}=\lambda\,\epsilon_{xx} \tag{29}$$

on the deformed region. Since there is no strain far behind the tip, this stress must be countered by the viscous force due to the movement of the displacement field

$$\lambda\,\epsilon_{xx}=\int\frac{\partial u_y}{\partial t}d\tilde{y}=-v\int\frac{du_y}{d\tilde{y}}d\tilde{y}=-v\Delta u_y. \tag{30}$$

Knowing how much u_y changes, we want to find its shape in the deformed region. Using $\partial_{\tilde{t}}u_y=0$ and $\partial_t u_y=-\delta\mathcal{F}/\delta u_y=(\lambda+2\mu)\partial_y^2 u_y$, we have

$$\frac{\partial}{\partial\tilde{t}}u_y=\frac{\partial u_y}{\partial t}+v\frac{\partial u_y}{\partial y}=(\lambda+2\mu)\frac{\partial^2 u_y}{\partial y^2}+v\frac{\partial u_y}{\partial y}=0. \tag{31}$$

A solution to this second-order differential equation apart from the crack tip position $y=vt$ is

$$u_y(y,t)=\begin{cases}\Delta u_y, & y<vt\\[2mm]\Delta u_y\exp\left[-\dfrac{v}{\lambda+2\mu}(y-vt)\right], & y>vt\end{cases} \tag{32}$$

where we used $u_y(\infty)=0$.

We can now find the energy dissipated due to the material deformation around the crack tip. Ignoring the phase-field in Eq. (10), our crude estimate gives the energy dissipated per unit length as the inverse velocity times the energy dissipated per unit time:

$$\left(\frac{\mathcal{F}}{\mathcal{Y}}\right)_{\text{diss}} = -\frac{1}{v}\frac{d}{dt}\mathcal{F} \approx \frac{\mathcal{X}}{v}\int_0^\infty \left(\frac{\partial u_y}{\partial t}\right)^2 d\tilde{y}$$

$$= \frac{\mathcal{X}}{v}\int_0^\infty \left[\frac{v^2 \Delta u_y}{\lambda + 2\mu}\exp-\left(\frac{v}{\lambda+2\mu}\right)\tilde{y}\right]^2 d\tilde{y}$$

$$= \frac{(\lambda \epsilon_{xx})^2 \mathcal{X}}{(\lambda+2\mu)2}, \tag{33}$$

where we used Eq. (30) in the last step. [To quadratic order in ϵ_{xx}, this equals $\lambda^2/4\mu(\lambda+2\mu)$ times $(\mathcal{F}/\mathcal{Y})_{\text{strain}}$, so the dissipation is a fixed fraction of the total available strain energy. For our system, the fraction is 1/8.] We thus conclude that the energy dissipated due to the deformation around the crack tip only depends on the initial strain and the width of the system. In our system of width $\mathcal{X}=200$, the strain corresponding to the fracture threshold is about $\epsilon_{xx}=0.026$. For numerical comparison, we insert the strain and the other values that we used in our simulations into Eq. (33), and find that $\mathcal{F}/\mathcal{Y}_{\text{diss}}\approx 0.07$, which is about twice the difference between $\mathcal{F}/\mathcal{Y}_{\text{strain}}$ and $\mathcal{F}/\mathcal{Y}_{\text{surface}}$. Even though we ignored both the phase-field ϕ and all variations in x, our crude estimate shows that as the velocity goes to zero a fixed fraction of the energy in front of the crack is used to strain the material in a diverging region around the crack tip before it is dissipated.

We also did a simulation to verify that Eq. (32) is of the right form. With $(\mathcal{X},\mathcal{Y})=(100,1200)$ and $\epsilon_{xx}=0.08$ [which gives $(\mathcal{F}/\mathcal{Y})_{\text{strain}}=1.01$], we did see an exponential decay of u_y in front of the crack tip. The numerical values were slightly off, with the exponential decay being twice as fast as predicted. This was to be expected since we have ignored the phase-field completely, which clearly couples to the displacement field at long distances. Our simulation area still was not long enough for Δu_y to saturate, but it reached about 2/3 of the value predicted in Eq. (30).

In Fig. 5, we plot the velocity as a function of strain energy available for fracture $(\mathcal{F}/\mathcal{Y})_{\text{strain}}$. In the fracture literature, the mode I fracture threshold is usually quoted in terms of the energy release rate [17]: the strain energy $\mathcal{G}$ flowing into the crack tip. This can be measured, for example, by the use of J integrals [18], see Appendix C.

From the discussion above, we conclude that the disparity between Griffith's prediction and the fracture threshold as measured by $(\mathcal{F}/\mathcal{Y})_{\text{strain}}$ is due to energy dissipation far from the crack. Thus we cannot expect $\mathcal{G}$ to equal $(\mathcal{F}/\mathcal{Y})_{\text{strain}}$. Indeed, the fracture threshold measured using a J integral close to the crack tip should agree with Griffith's prediction.

V. FUTURE WORK

Fracture often occurs in crystalline materials, and it therefore seems reasonable to add anisotropy to quantities such as mobility, surface tension, and elastic strain energy. There might also be unwanted anisotropy included due to the underlying grid in the numerical solver, and one might be able to repress this effect by adding ''counter'' anisotropy in the quantities mentioned above. In addition to anisotropy, one could add some noise; either spatially in the Hamiltonian or initial conditions, which would break the symmetry and add heterogeneities, or temporally, which would mimic the effects of fluctuations due to a finite temperature.

Because of the fourth-order gradients, our simulation is rather numerically intensive. Using a multiresolution grid would speed up the calculation [19]. The main idea is that additional information can be added between existing grid points where a linear interpolation would give poor results (that is, add grid points locally where the solution has high frequency components). This way one can achieve a solution with uniform accuracy and avoid unnecessary use of computational resources. A similar approach can be found in [20], where an adaptive mesh in a phase-field solidification problem is used to add detail only at the boundaries where it is needed.

Currently, the numerical integration of the phase-field equations is done partly using Fourier transforms. This allows us to do all the linear parts of the equations implicitly without solving huge linear systems. On the other hand, the current implementations put several limitations on the kinds of simulations that can be done. In particular, it is hard to do simulations without using periodic boundary conditions. It thus seems beneficial to use real-space implicit methods (and perhaps add in multiresolution capabilities at the same time).

This paper is only concerned with mode I fracture in two dimensions. It would seem reasonable to try to extend the model to include modes II and III as well. Mode II could be done either by shearing the model with a crack running vertical or horizontal, or by squeezing one way and extending the other with a strain s and 45° crack, where s is equal to the shear strain divided by $\sqrt{2}$. One way to start exploring mode II could be to use finite element calculations to get an initial sheared configuration, and then use the phase-field model to relax this system. Mode III has recently been explored in Ref. [5], where a different, nonconserved phase-field model is used. Ultimately, the goal is to do three-dimensional simulations incorporating all three modes of fracture, given the success of the two-dimensional models.

TABLE I. Relations between λ, μ, and ν when a material is stretched infinitesimally.

Dimension	ϕ'	$\mathcal{F}_0$	$\mathcal{F}_1$	$\mathcal{F}_2$
2	$\dfrac{hw}{h'w'}$	—	$\lambda = \dfrac{2\mu\nu}{1-\nu} - \dfrac{1}{2}$	$\lambda = \dfrac{2\mu\nu}{1-\nu}$
2	1	$\lambda = \dfrac{2\mu\nu}{1-\nu}$	$\lambda = \dfrac{2\mu\nu}{1-\nu}$	$\lambda = \dfrac{2\mu\nu+1}{1-\nu} - \dfrac{1}{2}$
3	1	$\lambda = \dfrac{2\mu\nu}{1-2\nu}$	$\lambda = \dfrac{2\mu\nu}{1-2\nu}$	$\lambda = \dfrac{2\mu\nu}{1-2\nu}$

Paul Dawson, and Nick Bailey for helpful comments and discussions.

APPENDIX A: REDUCED UNITS

Most of the equations in this paper are written in unitless form, where the basic units are

$$l = w/h \quad \text{(length)}, \tag{A1a}$$

$$f = h^2 \quad \text{(energy density)}, \tag{A1b}$$

$$d = 1/\eta \quad \text{(diffusivity)}. \tag{A1c}$$

Here w^2 is the cost of gradients of ϕ in Eq. (1), $h^2/64$ is the height of the energy barrier between the phases in Eq. (2), and η is the viscosity controlling the response of the displacement field in Eq. (8b). The equations were made unitless by replacing all quantities (say, x and t) by their unitless counterparts multiplied by the appropriate combination of basic units (as in $x*l$ and $t*l^2/fd$, $*=$ unitless), and then choosing the basic units l, f, and d conveniently. To transform the quantities back from unitless form, just multiply them with their basic unit ($x = x*l$).

As a reminder, the variational derivatives of the free energy and the Lamé constants λ and μ all have units of energy density f, and the diffusion constant D has units of diffusivity d.

APPENDIX B: LAMÉ CONSTANTS

We have to determine what the relation between λ, μ, and ν is in our model: the addition of ϕ changes the effective elastic constants on long wavelengths from the values input to the free energy in Eq. (5). In the following, two- (2D) and three-dimensional (3D) refer to the mathematical dimensionality of the system, not special cases like plain strain. Start with a rectangular sheet (2D) or block (3D) of material, with height h in the y direction, and width w in the x direction (and in the z direction if it is in 3D). The idea is then to strain the material by an infinitesimal amount in the y direction until the height becomes h', and minimize the free energy with respect to the new width w'. The Poisson ratio ν is then given by

$$\nu = \lim_{h' \to h} \left(-\frac{\epsilon_{xx}}{\epsilon_{yy}} \right). \tag{B1}$$

Before doing the model proper, we start off with a free energy that *only* includes the elastic energy

$$\mathcal{F}_0 = \int_V dV \, \mathcal{E}[\epsilon]. \tag{B2a}$$

In the scenario that is described above there is no shear, so $\epsilon_{ij} = 0$ if $i \neq j$. Further, $\epsilon_{yy} = (h'-h)/h'$, and $\epsilon_{xx} = \epsilon_{zz} = (w'-w)/w'$ (in 2D, ϵ_{zz} is nonexistent). The integrand is constant everywhere, so the integral turns into a factor $h'(w')^2$ (or $h'w'$ in 2D). This is inserted into Eq. (B2a). Next, one finds the minimum of $\mathcal{F}_0$ with respect to w' (keeping all the other variables constant), and inserts it into Eq. (B1), taking the limit. Solving for λ does indeed give the standard answers for both two and three dimensions.

The next two energies that were tried were

$$\mathcal{F}_1 = \int_V dV \frac{1}{4} \phi^2 (\phi-1)^2 + \phi^2 \mathcal{E}[\epsilon], \tag{B2b}$$

$$\mathcal{F}_2 = \int_V dV \frac{1}{4} \phi^2 (\phi - \phi_s[\epsilon])^2 + \phi^2 \mathcal{E}[\epsilon]. \tag{B2c}$$

The gradient term is zero, since ϕ is uniform. Having introduced ϕ, we need to add another restriction: conservation of mass is given by $\phi_0 hw^2 = \phi'h'(w')^2$ (or $\phi_0 hw = \phi'h'w'$ in 2D). Here, ϕ_0 is the value when the material is relaxed, while ϕ' is the value after the material has been stretched [it is the latter which will be inserted into Eqs. (B2b) and (B2c)]. We assume that $\phi_0 \equiv 1$. We checked two cases for ϕ': one where $\phi' \equiv 1$ (the density was not allowed to change), and one where $\phi' = hw/h'w'$ (the latter is the 2D expression; having ϕ change in three dimensions was quite hard to calculate).

The results after minimizing the free energy, finding ν, taking the limit, and solving for λ can be found in Table I. As one can see, adding the phase-field ϕ to the model also requires that the double-well potential includes the ϵ_{mm} term (through $\phi_s[\epsilon]$) in order to get the right relation between material constants.

A final comment: The model described in this paper is two dimensional, so the maximum range for the Poisson ra-

tio in two dimensions is $0<\nu<1$. This is *equivalent* to a three-dimensional model under plain strain, where the corresponding range for the Poisson ratio is $0<\nu<1/2$. Thus the latter expression (for three-dimensional plain strain) is used throughout the paper, often using the value $\nu=1/3$.

APPENDIX C: THE J INTEGRAL

The energy release rate $\mathcal{G}$ can be calculated for our problem (where the crack is parallel to the y axis) using the J_y component of the J integral. Instead of performing the line integral, it is common to convert it to an area integral for increased accuracy when doing the integral numerically. The area integral is defined as

$$J_y = -\int_A \Omega(x,y) dx\, dy, \qquad (C1)$$

where

$$\Omega(x,y) = \mathcal{E}[\epsilon]\frac{\partial q}{\partial y} - \sigma_{ij}\frac{\partial u_i}{\partial y}\frac{\partial q}{\partial x_j}. \qquad (C2)$$

Here q is a function that is unity around the crack tip and zero outside. Notice that if q is constant in a region, then $\Omega(x,y) \equiv 0$, and in effect the line integral is replaced by a "thick line" integral, where the thick line exists everywhere q has a gradient.

A small complication is that our $\Omega(x,y)$ is given in deformed coordinates $\xi_x(x,y) \equiv x + u_x(x,y)$ and $\xi_y(x,y) \equiv y + u_y(x,y)$:

$$J_y = -\int_{\tilde{A}} \tilde{\Omega}(\xi_x,\xi_y)|\mathcal{J}(\xi_x,\xi_y)|d\xi_x\,d\xi_y, \qquad (C3)$$

where $\mathcal{J}$ is the Jacobian given by

$$\mathcal{J}(\xi_x,\xi_y) = \begin{bmatrix} \dfrac{\partial x}{\partial \xi_x} & \dfrac{\partial x}{\partial \xi_y} \\[2mm] \dfrac{\partial y}{\partial \xi_x} & \dfrac{\partial y}{\partial \xi_y} \end{bmatrix}. \qquad (C4)$$

Using the identity $\mathcal{J}(\xi_x,\xi_y)\cdot\mathcal{J}(x,y)=I$, one gets

$$|\mathcal{J}(\xi_x,\xi_y)| = \frac{1}{|\mathcal{J}(x,y)|} = \frac{1}{\partial_x\xi_x\partial_y\xi_y - \partial_y\xi_x\partial_x\xi_y}$$

$$= \frac{1}{(1+\epsilon_{xx})(1+\epsilon_{yy}) - \partial_y u_x\partial_x u_y}. \qquad (C5)$$

The energy release rate can thus easily be computed using Eq. (C3), where ξ_x and ξ_y are the usual coordinates on the phase-field grid.

---

[1] J. A. Hodgdon and J. P. Sethna, Phys. Rev. B **47**, 4831 (1993).

[2] R. G. Pettit, C.-S. Chen, A. R. Ingraffea, and C. Y. Hui, Eng. Fract. Mech. **68**, 1181 (2001).

[3] See e.g., J. S. Langer, Rev. Mod. Phys. **52**, 1 (1980); J. A. Warren, IEEE Comput. Sci. Eng. **2**, 38 (1995); A. Karma and W.-J. Rappel, Phys. Rev. E **57**, 4323 (1998); Y.-T. Kim, N. Provatas, N. Goldenfeld, and J. Dantzig, *ibid.* **59**, R2546 (1999).

[4] I. S. Aranson, V. A. Kalatsky, and V. M. Vinokur, Phys. Rev. Lett. **85**, 118 (2000) (mode I fracture simulation, nonconserved order parameter, elastic energy multiplied by ϕ).

[5] A. Karma, D. A. Kessler, and H. Levine, Phys. Rev. Lett. **87**, 045501 (2001) (mode III fracture simulation, nonconserved order parameter).

[6] J. Muller and M. Grant, Phys. Rev. Lett. **82**, 1736 (1999) (surface instabilities induced by stress, nonconserved order parameter, elastic energy multiplied by a quartic polynomial, quadratic near $\phi=0$).

[7] K. Kassner and C. Misbah, Europhys. Lett. **46**, 217 (1999); K. Kassner, C. Misbah, J. Muller, J. Kappey, and P. Kohlert, Phys. Rev. E **63**, 036117 (2001); J. Cryst. Growth **225**, 289 (2001) (solid-liquid instabilities induced by stress, nonconserved order parameter, elastic energy multiplied by a cubic polynomial, quadratic near $\phi=0$).

[8] D. N. Bhate, A. Kumar, and A. F. Bower, J. Appl. Phys. **87**, 1712 (2000) (electromigration simulations under strain, showing void growth similar to fracture, conserved order parameter, elastic energy multiplied by ϕ, phase-field energy modified to force constant ϕ outside neighborhood of interface).

[9] L. D. Landau and E. M. Lifshitz, *Theory of Elasticity*, translated by J. B. Sykes and W. H. Reid (Pergamon, Oxford, 1970), p. 2.

[10] If we had chosen a nonzero constant of integration in Eq. (14), then Eq. (15) would not have been linear in ϕ, and $T[\phi]$ would not have been a simple fourth-order polynomial.

[11] For easy reference, this means that $\lambda + 2\mu = B^2/(1-2B^2)$, and if $\lambda=2\mu=2$ then $B=\pm2/3$.

[12] We use an operator splitting method, that alternates nonlinear steps in real space and gradient steps in Fourier space [W. H. Press, S. A. Teukolsky, W. T. Vetterling, and B. P. Flannery, *Numerical Recipes in C*, 2nd ed. (Cambridge University Press, Cambridge, 1992), Sec. 19.3]; for a more systematic method, see D. J. Eyre, *Computational and Mathematical Models of Microstructural Evolution*, edited by J. W. Bullard, R. Kalia, M. Stoneham, and L.-Q. Chen (The Materials Research Society, Pittsburgh, PA, 1998).

[13] L. O. Eastgate, J. P. Sethna, M. Rauscher, T. Cretegny, C.-S. Chen, and C. R. Myers, http://www.arXiv.org; e-print cond-mat/0108249v1 (version 1).

[14] A. A. Griffith, Philos. Trans. R. Soc. London, Ser. A **221**, 163 (1921).

[15] $\phi = 0$ is also a local minimum of the free energy density, but this corresponds to the gas phase.

[16] After relaxing the interface numerically, the actual value of the surface energy is $(\mathcal{F}/\mathcal{Y})_{\text{surface}} = 0.219 \pm 10^{-5}$. The reason it is not 2/9 is that the numerical solution is slightly different from the analytical one due to the discrete nature of the simulation.

[17] For plane strain, the fracture threshold is given in terms of the stress intensity factor K_I, which is related to the energy release rate by $\mathcal{G} = K_I^2 (1 - \nu)/2\mu$.

[18] J. R. Rice, *Mathematical Fundamentals*, edited by H. Liebowitz (Academic, New York, 1968), Vol. 2, p. 191.

[19] T. A. Arias, Rev. Mod. Phys. **71**, 267 (1999).

[20] N. Provatas, N. Goldenfeld, and J. Dantzig, Phys. Rev. Lett. **80**, 3308 (1998).